

SUPPORTING INFORMATION

Fluorescent probe based on pyrazoline with significant Stokes shifts for the detection of Cu²⁺ ion and its applications

Yajing Shang*, Xinghu Wu, Haoting Luo

School of Chemistry and Chemical Engineering, Lanzhou Jiaotong University,

Lanzhou, 730070, China

*Corresponding authors.

E-mail addresses: shangyaj@mail.lzjtu.cn

Table of Contents

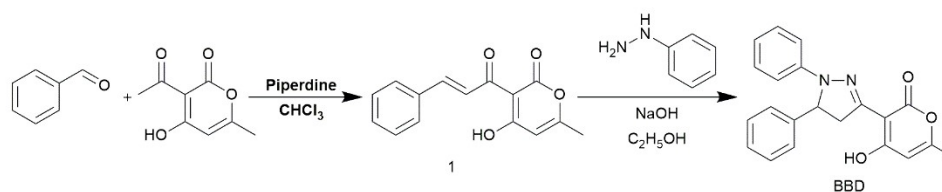
1. Experimental section	2
1.1 Materials and instruments	2
1.2 Synthesis of compound	2
1.3 Spectrophotometric measurements	3
1.4 Determination of relative quantum yield	3
1.5 Cell Culture	3
1.6 MTT assay	3
1.7 Imaging of Cu ²⁺ in Living Cells and zebrafish	3
2. ¹ H NMR, ¹³ C NMR and ESI-MS	4
4. Figure	5
5. Reference	10

1. Experimental section

1.1 Materials and instruments

The reagents and drugs utilized in this study primarily consist of commercially sourced dehydroacetic acid, benzaldehyde, trichloromethane, ethanol, benzoquinone, glacial acetic acid, dimethyl sulfoxide (DMSO), etc., which were employed without further purification. All solvents used in this research were of analytical grade. The reaction progress was monitored using thin-layer chromatography (TLC) and observed under a UV lamp at either 254 nm or 365 nm. Proton nuclear magnetic resonance (^1H NMR) and carbon-13 nuclear magnetic resonance (^{13}C NMR) spectra were acquired on a Brook AVIII-500 MHz spectrometer at 25°C. Chemical shifts for both ^1H NMR and ^{13}C NMR were referenced to the residual solvent peak (CDCl_3 : $\delta = 7.27$ ppm; DMSO-d_6 : $\delta = 2.5$ ppm). Data were reported as follows: chemical shift, multiplicity (s = singlet, d = doublet, t = triplet, m = multiplet), coupling constant (Hz), and integral value. Fluorescence spectra were recorded using an F97pro fluorescence spectrophotometer while UV-visible spectra were obtained with a Thermo BioMate 3S UV/visible spectrophotometer. Melting points were determined utilizing an XD-4 digital micromelting point instrument. Infrared spectra spanning the range of 4000-400 cm^{-1} and electrospray ionization mass spectrometry (ESI-MS) data were collected employing a VERTEX 70 Fourier transform infrared spectrophotometer and Q-Exactive mass spectrometer respectively.

1.2 Synthesis of compound



Scheme 1. Synthesis of compound BBD

Synthesis of compound 1

The synthesis of chalcone 1 was conducted following the procedure described in literature ¹.

Synthesis of BBD (3-(1,5-diphenyl-4,5-dihydro-1H-pyrazol-3-yl)-4-hydroxy-6-methyl-2H-pyran-2-one)

Combine chalcone 1 (0.3469g, 1mmol), phenyl hydrazine (0.1081g, 1mmol), and NaOH (0.004g, 0.1mmol) with anhydrous ethanol and stir the mixture for 12 hours under reflux conditions. Subsequently, remove a portion of the ethanol via reduced pressure evaporation and introduce 50 ml of distilled water. Adjust the pH to neutral by adding dilute hydrochloric acid, resulting in the formation of a yellow precipitate. Filter the mixture, wash it with water, dry thoroughly, and purify through column chromatography to obtain a solid product exhibiting a yellow coloration. ^1H NMR (500 MHz, CDCl_3) δ 13.35 (s, 1H), 7.37 - 7.23 (m, 6H), 7.19 (dd, $J = 8.7, 7.2$ Hz, 1H), 6.88 (s, 1H), 6.87 - 6.80 (m, 2H), 6.04 (s, 1H), 5.13 (dd, $J = 12.3, 8.0$ Hz, 1H), 4.16 (dd, $J = 18.9, 12.3$ Hz, 1H), 3.49 (dd, $J = 18.9, 8.0$ Hz, 1H), 2.26 (s, 3H), 1.57 (s, 1H). ^{13}C NMR (126 MHz, CDCl_3) δ 170.56, 163.22, 149.83, 144.15, 141.86, 129.17, 127.74, 125.87, 120.01, 113.23, 101.10, 63.41, 46.37, 20.19.

1.3 Spectrophotometric measurements

The metal ion stock solutions (5 mM) were prepared by dissolving various metal salts in deionized water, including Ag⁺, Al³⁺, Ba²⁺, Ca²⁺, Cd²⁺, Co²⁺, Cr³⁺, Cu²⁺, Fe³⁺, Hg²⁺, K⁺, Mg²⁺, Mn²⁺, Na⁺, Ni²⁺, Pb²⁺ and Zn²⁺. The probe BBD stock solution (5 mM) was prepared by dissolving the probe BBD in DMSO. For UV and fluorescence emission spectroscopy experiments, 20 µl of probe BBD and 20 µl of the respective metal ion stock solutions were added to ethanol/Hepes buffer (1:1, v/v), resulting in a final volume of 2 ml. In the fluorescence measurement, the excitation and emission wavelengths were set at 398 nm and 520 nm, respectively. The excitation and emission slit widths were adjusted to 10 nm.

1.4 Determination of relative quantum yield

The fluorescence quantum yield of the sample in ethanol is determined by relative measurement method. The quantum yield is calculated using the following formula:

$$\Phi_{F(X)} = \Phi_{F(S)} \times \left(\frac{A_S \times F_X}{A_X \times F_S} \right) \left(\frac{n_X}{n_S} \right)^2$$

Φ_F : Fluorescence quantum yield, S/X: standard / test, A_S/A_X : The absorbance of the standard / test solution, F_S / F_X : Integrated area of fluorescence for solutions of standards / test, n: The refraction coefficient of different solvents.

The absorbance of the test sample and the standard sample at their respective maximum absorption points is controlled to be below 0.05. The standard sample is Rhodamine B, which has a fluorescence quantum yield of 0.89 in ethanol.

1.5 Cell Culture

The HeLa cells (human cervical cancer cells) were utilized as the experimental model in this study. These cells were cultured in DMEM medium supplemented with 10% FBS and 1% penicillin-streptomycin mixture, followed by incubation at 37°C under a controlled atmosphere of 5% CO₂.

1.6 MTT assay

The HeLa cells were seeded in 96-well plates at a density of $7 \times 10^4 \text{ L}^{-1}$ and incubated for 24 hours. Subsequently, the old medium was replaced with fresh medium (100 µL) containing varying concentrations of probes. The cells were further incubated for an additional 12 hours. Following this, a mixture of MTT and medium (1:9) (110 µL) was added to each well and incubated for 4 hours. After discarding the mixture, DMSO (100 µL) was added to each well. The absorbance at 570 nm was measured using a Thermo (Multiskan MK3) microplate reader. Finally, the percentage of cell viability was calculated relative to the control well designated as having 100% live cells.

1.7 Imaging of Cu²⁺ in Living Cells and zebrafish

Imaging of exogenous Cu²⁺ cell probes was studied. In the first group, cells were incubated with PBS buffer for 30 min. In the second group, cells were incubated with BBD (30 µM) for 30 min. In the third group, cells were first incubated with Cu²⁺ (100 µM) for 30 min, and then treated with BBD (30 µM) for 30 min. Fluorescence images of the cells were obtained by confocal laser scanning microscopy.

The probe was imaged in zebrafish. In the first group, zebrafish were incubated with PBS buffer for 30 minutes. In the second group, zebrafish were incubated with BBD (20 µM) for 30 minutes. In the third group, zebrafish were incubated with Cu²⁺ (100 µM) for 30 minutes, followed by

incubation with BBD (20 μM) for 30 minutes. Fluorescent images of zebrafish were obtained using a confocal laser scanning microscope.

2. ^1H NMR, ^{13}C NMR and ESI-MS

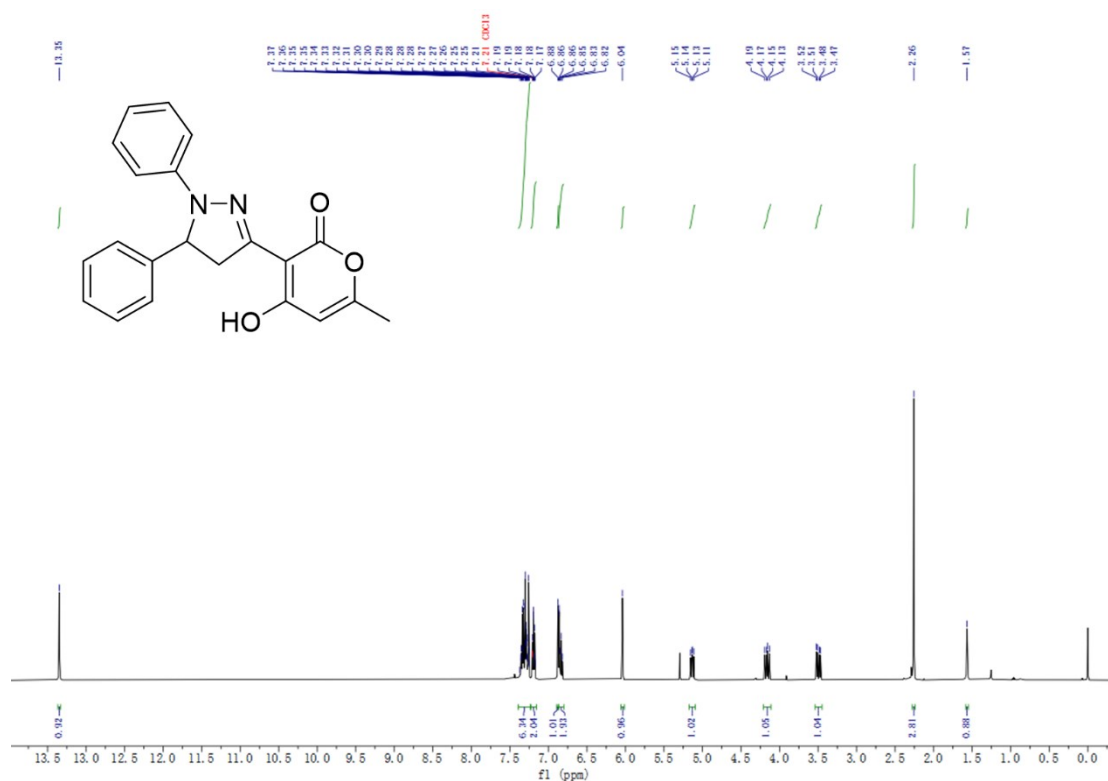


Fig. S1 ^1H NMR spectrum of probe BBD in CDCl_3 at room temperature.

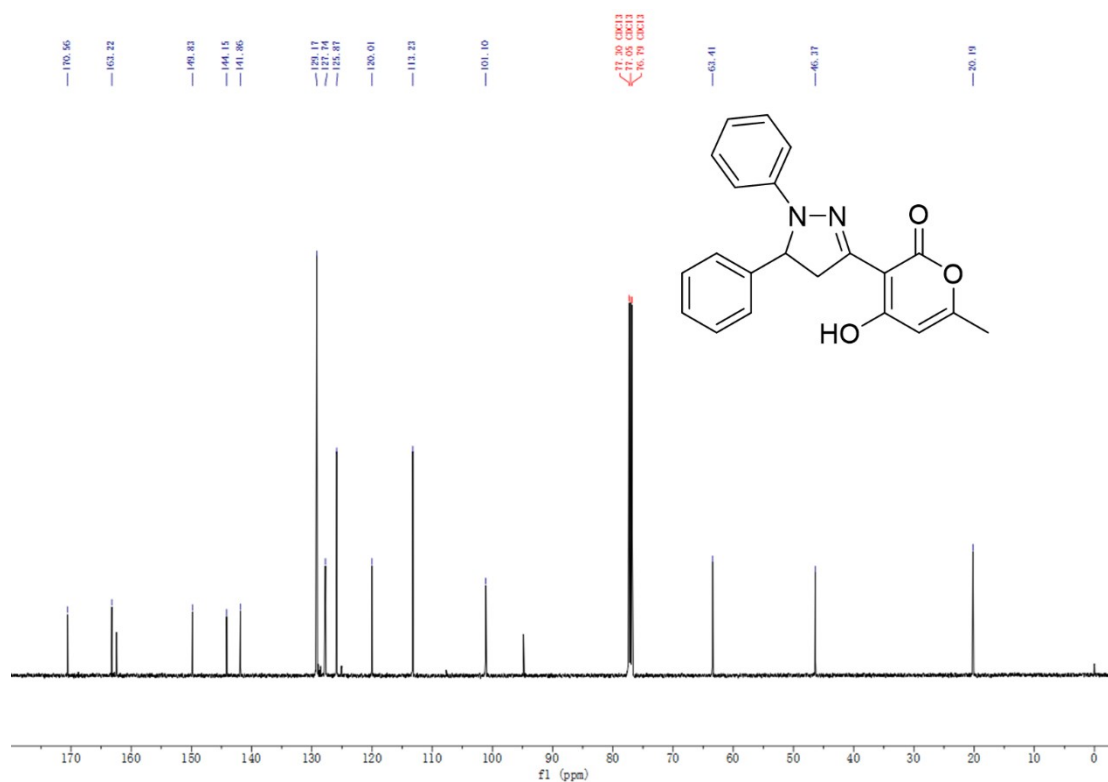


Fig. S2 ^{13}C NMR spectrum of probe BBD in CDCl_3 at room temperature.

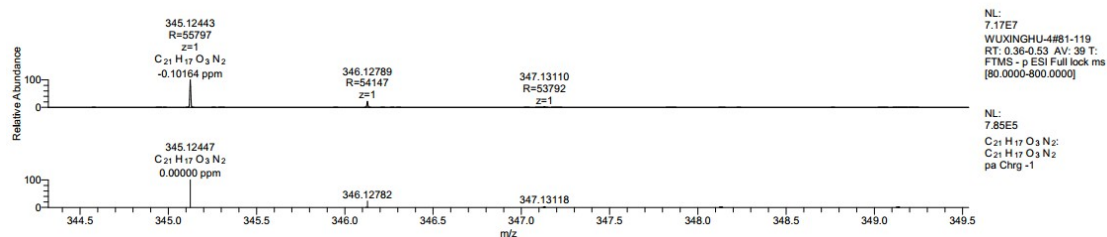


Fig. S3. ESI-MS spectrum of probe [BBD-H⁺].

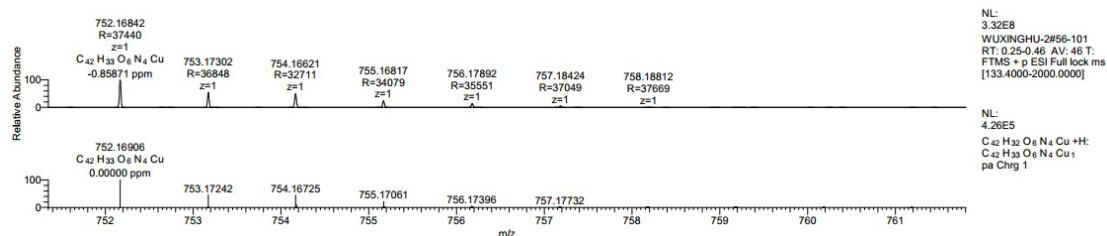


Fig. S4 ESI-MS spectrum of probe [2(BBD-H⁺) + Cu²⁺ - 2H⁺].

4. Figure

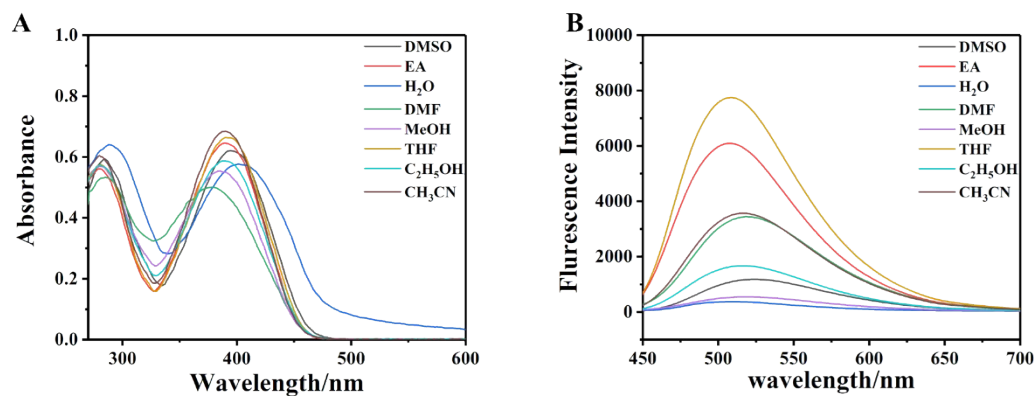


Fig. S5 A) UV spectra of probes in different solvents; B) Fluorescence spectra of probes in different solvents.

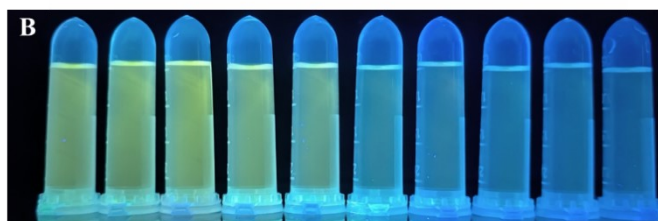
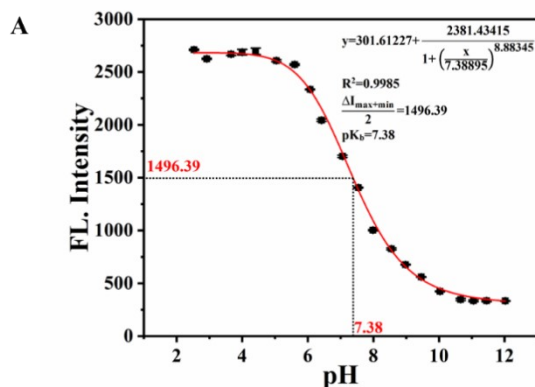


Fig. S6 A) The fluorescence intensity of compound BBD (20 μM , $\lambda_{\text{ex}} = 398 \text{ nm}$) at different pH values (2.5-12). B) Fluorescence color images of compound BBD (20 μM) at different pH values (3-12).

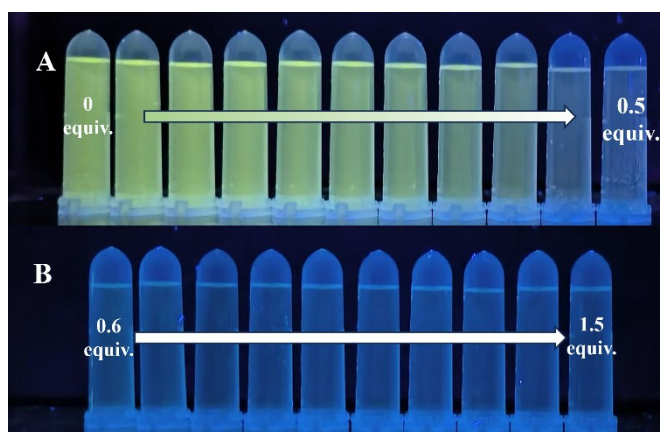


Fig. S7 Under 364 nm UV light, the fluorescence color images of the probe (50 μM) in different concentrations of Cu^{2+} solution.

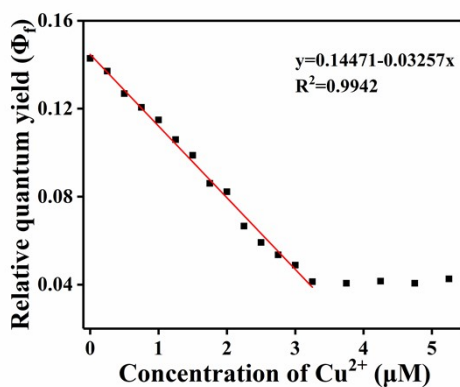


Fig. S8 Relative fluorescence quantum yield of probe BBD.

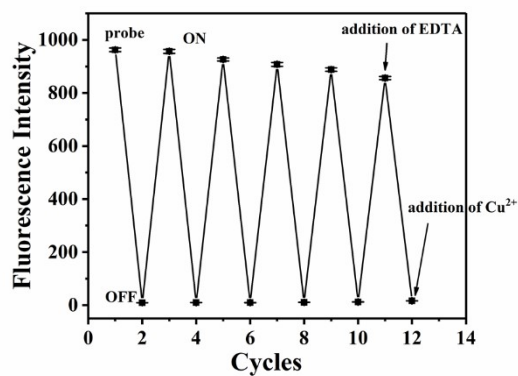


Fig. S9 Fluorescence intensity of probe BBD when alternately adding 1 equivalent of Cu^{2+} and EDTA.

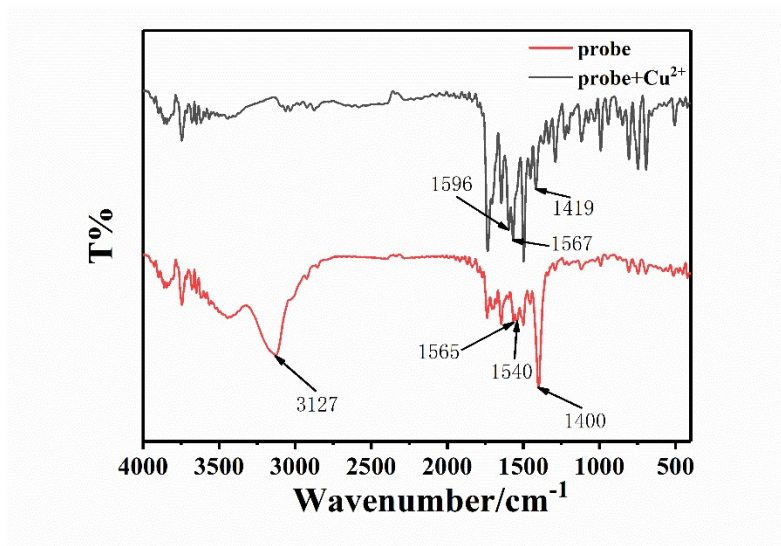


Fig. S10 Infrared spectra of probe BBD and its complexes with Cu^{2+} ions.

Table S1. Comparison with previously reported Cu²⁺ fluorescent probes.

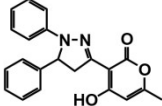
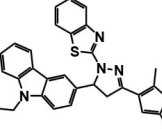
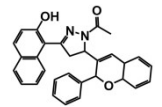
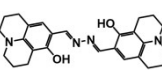
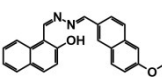
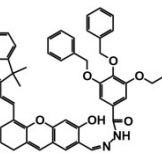
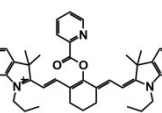
Probe	$\lambda_{ex}/\lambda_{em}$	Time	solvent system	LOD	Application	Reference
	398 nm/520 nm	20s	Ethanol/H ₂ O (1:1, V/V)	8.62×10^{-7} M	Hela cells zebrafish	This work
	335nm/ 408- 432 nm	-	DMF/H ₂ O (9:1, V/V)	-	-	2
	275 nm/417 nm	-	Ethanol/H ₂ O (1:1, V/V)	8.85×10^{-7} M	PK-21 cells	3
	492nm/ 519nm	≤1min	H ₂ O/DMSO (1:5, V/V)	2.5×10^{-7} M	Real water sample Test strips	4
	423nm/ 535nm	-	Hepes	2.9×10^{-8} M	Test strips Wine and beer	5
	730nm/ 810nm	60s	H ₂ O/DMSO (99:1, V/V)	0.54×10^{-6} M	H22 cell H22 tumor bearing mice	6
	792nm/ 810nm	40min	HEPES(containin g 0.1% CrEL)	0.53×10^{-7} M	SH-SY5Y cells Arabidopsis Roots Neuroblastoma Tumors In vivo	7

Table S2. Optimized bond lengths and angles for the excited states of BBD and BBD-Cu²⁺.

BBD		TD-DFT/B3LYP/6-31G (d, p)		BBD-Cu ²⁺		TD-DFT/B3LYP/lanl2dz	
Bond length (Å)		Bond Angle (°)		Bond length (Å)		Bond Angle (°)	
C1-C2	1.54773	C1-C2-N6	101.63071	C1-C2	1.55463	C1-C2-N6	101.18186
C1-C7	1.50864	C2-N6-N5	112.65119	C1-C7	1.52804	C2-N6-N5	111.96214
C2-N6	1.47128	N6-N5-C7	106.86213	C2-N6	1.48617	N6-N5-C7	109.21139
C7-N5	1.33081	C1-C7-N5	113.19091	C7-N5	1.34321	C1-C7-N5	110.72106
N5-N6	1.43002	C7-C1-C2	103.02763	N5-N6	1.40957	C7-C1-C2	103.67356
N6-C8	1.34311	N5-C7-C19	121.34366	N6-C8	1.40110	N5-C7-C19	125.19508
C8-C9	1.43396	C1-C7-C19	125.46168	C8-C9	1.42067	C1-C7-C19	124.07794
C8-C10	1.43481	C7-C19-C20	121.25195	C8-C10	1.41860	C7-C19-C20	123.20887
C9-C11	1.38106	C7-C19-C21	119.46428	C9-C11	1.40283	C7-C19-C21	117.66540
C10-C13	1.38383	C19-C20-C22	119.61086	C10-C13	1.40355	C19-C20-C22	118.59126
C13-C15	1.40409	C20-C22-C23	120.12809	C13-C15	1.41033	C20-C22-C23	121.68638
C15-C11	1.40876	C22-C23-O40	121.15465	C15-C11	1.41167	C22-C23-O39	120.03915
C7-C19	1.42176	C23-O40-C21	122.62611	C7-C19	1.44188	C23-O39-C21	123.04782
C19-C21	1.43960	O40-C21-C19	117.18645	C19-C21	1.45414	O39-C21-C19	117.42589
C21-O40	1.40551	C19-C21-O25	127.50303	C21-O39	1.43372	C19-C21-O25	128.59330
O40-C23	1.37360	O25-C21-O40	115.30873	O39-C23	1.39121	O25-C21-O39	113.97698
C23-C22	1.37787	O40-C23-C26	112.16651	C23-C22	1.35971	O39-C23-C26	112.35802
C20-C22	1.39788	C22-C23-C26	126.67523	C20-C22	1.45485	C22-C23-C26	127.60137
C19-C20	1.44927	C19-C20-O30	122.15453	C19-C20	1.44889	C19-C20-O30	123.78635
C21-O25	1.22271	C22-C20-O30	118.18718	C21-O25	1.25226	C22-C20-O30	117.62072
C20-O30	1.34915	C2-C33-C34	121.40901	C20-O30	1.30029	C2-C32-C33	121.85139
C23-C26	1.48732	C33-C34-C35	120.27549	C23-C26	1.49670	C32-C33-C34	120.02925
C2-C33	1.52490	C34-C35-C37	120.32488	C2-C32	1.53156	C33-C34-C36	120.45735
C33-C34	1.40161	C35-C37-C41	119.65377	C32-C33	1.41101	C34-C36-C40	119.57760
C34-C35	1.39627	C37-C41-C43	120.02262	C33-C34	1.40913	C36-C40-C42	120.02844
C35-C37	1.39816	C41-C43-C33	120.57385	C34-C36	1.40914	C40-C42-C32	120.48127
C37-C41	1.39678	C43-C33-C2	119.41219	C36-C40	1.40994	C42-C32-C2	118.68146
C41-C43	1.39756	C2-N6-C8	127.23758	C40-C42	1.40767	C2-N6-C8	125.09288
C43-C33	1.40058	N5-N6-C8	120.00940	C42-C32	1.41213	N5-N6-C8	121.85680
		N6-C8-C9	121.01824	N5-Cu87	2.06257	N6-C8-C9	119.59311
		C8-C9-C11	119.94869	O30-Cu87	2.05686	C8-C9-C11	119.92284
		C9-C11-C15	121.05453			C9-C11-C15	120.83556
		C11-C15-C13	119.42611			C11-C15-C13	119.16467
		C15-C13-C10	121.08443			C15-C13-C10	120.64124
		C13-C10-C8	119.88008			C13-C10-C8	120.15769
		C10-C8-N6	120.38339			C10-C8-N6	121.13551
		C10-C8-C9	118.59794			C10-C8-C9	119.24417
						C7-N5-Cu87	126.53676
						N6-N5-Cu87	120.76052
						C20-O30-Cu87	130.01361

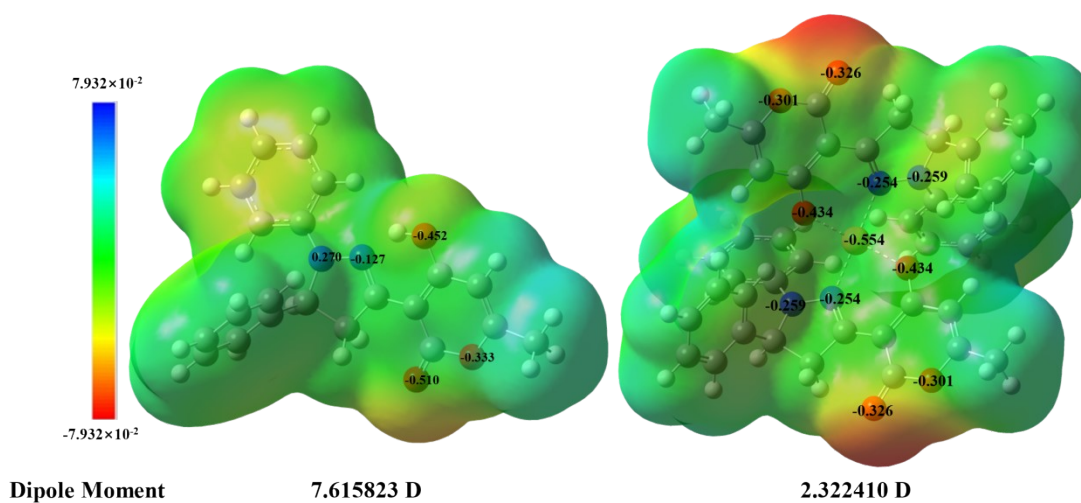


Fig. S11 Electrostatic potential diagram of BBD and BBD-Cu²⁺.

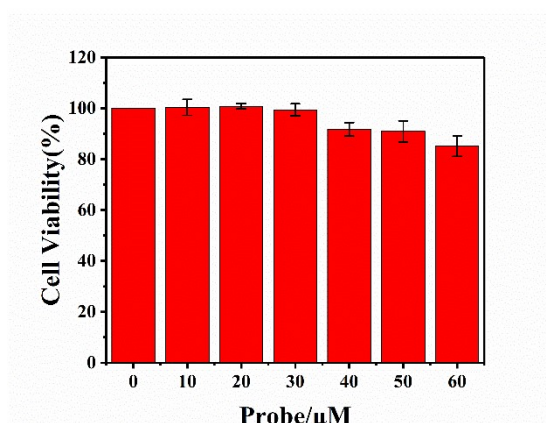


Fig. S12 Hela cells were incubated with different concentrations of BBD probes for 12 hours, and the cell viability was evaluated (%).

5. Reference

1. Y.J. Shang, Y.Y. Li, X.H. Wu, J. Li, A novel pyrazoline-based turn-on fluorescent probe for highly sensitive detection of Al³⁺ in aqueous solution and its applications, Chem. Pap. 78 (2024) 1659–1670, <https://doi.org/10.1007/s11696-023-03193-5>.
2. A.M. Asiri, N.S.M. Al-Ghamdi, H. Dzudzevic-Cancar, P. Kumar, S.A. Khan, Physicochemical and Photophysical investigation of newly

- synthesized carbazole containing pyrazoline-benzothiazole as fluorescent chemosensor for the detection of Cu^{2+} , Fe^{3+} & Fe^{2+} metal ion, *J. Mol. Struct.* 1195 (2019) 670-680, <https://doi.org/10.1016/j.molstruc.2019.05.088>.
3. Y.P. Zhang, Y.C. Zhao, Q.H. Xue, Yu.S. Yang, H.C. Guo, J.J. Xue, A novel pyrazoline-based fluorescent probe for Cu^{2+} in aqueous solution and imaging in live cell, *Inorg. Chem. Commun.* 129 (2021) 108612, <https://doi.org/10.1016/j.inoche.2021.108612>.
 4. A. Maiti, S. Ahamed, M. Mahato, et al. A Julolidine Coupled Azine-based Reversible Chromo-fluorogenic Probe for Specific Detection of Cu^{2+} Ions, *J Fluoresc* (2024). <https://doi.org/10.1007/s10895-023-03577-6>.
 5. H. Hu, L. Xue, Y.L. Yao, L.L. Deng, H.B. Wang, A novel fluorescent probe used for the detection of Cu^{2+} in water system with AIE properties, *J. Mol. Struct.* 1315 (2024) 138878, <https://doi.org/10.1016/j.molstruc.2024.138878>.
 6. T. Zhang, H.R. Chi, Guo, J.J. Guo, X.M. Lu, G.L. Li, Construction of a Cu^{2+} -Responsive NIR Fluorescent Probe and the Preliminary Evaluation of its Multifunctional Application, *J. Fluoresc*, (2024). <https://doi.org/10.1007/s10895-024-03610-2>.
 7. J.P. Zhu, Marcus E. Graziotto, Veronica Cottam, Tom Hawtrey, Liam D. Adair, Benjamin G. Trist, Nguyen T.H. Pham, Jourdin R. C.

Rouaen, Carolyn Ohno, Marcus Heisler, Orazio Vittorio, Kay L. Double, Elizabeth J. New, Near-Infrared Ratiometric Fluorescent Probe for Detecting Endogenous Cu²⁺ in the Brain, ACS Sens, 9 (2024) 2858–2868. <https://doi.org/10.1021/acssensors.3c02549>.